Tension Stiffening and Crack Formation in Reinforced Concrete Members with Fiber-Reinforced Polymer Sheets

Yuichi Sato[1] and Frank J. Vecchio, M.ASCE[2]

Abstract: Models to estimate crack spacings and tension stiffening effects in reinforced concrete (RC) members with externally bonded fiber-reinforced polymer (FRP) sheets are presented. Due to the lack of experimental evidence on the tension stiffening effect of FRP sheeting, a theoretical approach based on the concept of tension chords is introduced. Crack formation and the tension stiffening of tension chords with FRP sheets are subjected to parametric analyses using bond stress-slip relations. The analytical results are then reduced into simple model equations. In addition to the FRP sheet, the bond characteristics between steel bars and concrete is also modeled according to a concept of average bond. These models are incorporated into the distributed stress field model, enabling reasonable estimations of the crack widths and the tension stiffening effects in RC members with the FRP sheets.

DOI: 10.1061/(ASCE)0733-9445(2003)129:6(717)

CE Database subject headings: Concrete, reinforced; Cracking; Sheets; Tension; Fiber-reinforced polymers.

Introduction

In recent years, there has been an increased need for strengthening or rehabilitation of reinforced concrete (RC) structures. An effective method for increasing the capacity of RC beams is through the use of externally bonded fiber-reinforced polymers (FRP). As the effectiveness of the FRP sheets has been widely recognized, reliable analytical methods are now required to simulate the response of strengthened or repaired RC. FRP sheets differ from conventional steel reinforcing bars with respect to the following three mechanical characteristics:

1. FRP sheets are elastic materials. Plastic deformation cannot be expected in their usage;
2. The ratio of the bonded area with concrete, relative to the cross-sectional area of the FRP sheet, is significantly larger than those of the conventional steel bars. The bond stress between the FRP and concrete therefore causes a remarkable increase in local stress of the FRP at cracks and often results in rupture without any plastic deformation; and
3. The FRP can peel off from the surfaces of the concrete. The peeling is a phenomenon similar to bond deterioration between steel bars and concrete, but occurs in a much more brittle manner.

These characteristics require special consideration when modeling the bonded interface and tension stiffening effect of the FRP.

Another important aspect of the FRP sheet is its contribution to crack formation in concrete. Despite a very brittle bond characteristic, the tensile stress induced by the bond contributes to the crack formation to a certain extent. Previous experimental work indicated that crack spacings in RC members became smaller when the members were jacketed with the FRP sheets (Sato et al. 1997a).

Recently, Vecchio developed the distributed stress field model (DSFM, Vecchio 2000) as an extension of the modified compression field theory (Vecchio and Collins 1986). The DSFM is mainly aimed at redevelopment of equilibrium and compatibility formulations based on considerations for slip distortions at cracks, unequal inclinations of principal stresses, and principal strains and degree of compression softening of concrete. The DSFM was adopted in a nonlinear finite-element method and was shown to provide accurate calculations. It should be emphasized that the DSFM enables the estimate of local stresses of reinforcements, at cracks, based on a consideration of tension stiffening effects. As described above, the mechanical characteristics of FRP are not identical to those of steel bars. Nevertheless, there is no difference between the FRP and the steel in terms of equilibrium and compatibility strain conditions of the bonded interface between concrete and the reinforcements. Therefore, modeling the tension stiffening effect and the crack formation in the RC with the FRP sheets can be rationally achieved in the DSFM as long as constitutive law of the bond is adequately considered.

After a brief review of the formulation and modeling of tension stiffening effects in the DSFM, this paper will present experimental examples of the bond characteristics between the FRP and concrete. Based on the local bond constitutive law, the tension stiffening effect of the FRP will then be analyzed. This study leads to simple models for the tension stiffening effect of FRP (as well as conventional steel bars) and their contribution to the crack formation of concrete. The models are corroborated in example analyses of beams with the FRP sheets.

Consideration of Tension Stiffening and Crack Formation in Distributed Stress Field Model

In the DSFM, Eq. (1) relates the average tensile concrete stress f_{c1m}, average reinforcement stress f_{sm}, and the local reinforcement stress at crack f_{scr}.

[1]Instructor, Dept. of Urban Environment Engineering, Kyoto Univ., Kyoto 606-8501, Japan. E-mail: satou@archi.kyoto-u.ac.jp

[2]Professor, Dept. of Civil Engineering, Univ. of Toronto, Toronto ON, Canada M5S 1A4.

Note. Associate Editor: Dat Duthinh. Discussion open until November 1, 2003. Separate discussions must be submitted for individual papers. To extend the closing date by one month, a written request must be filed with the ASCE Managing Editor. The manuscript for this paper was submitted for review and possible publication on October 25, 2001; approved on July 29, 2002. This paper is part of the ***Journal of Structural Engineering***, Vol. 129, No. 6, June 1, 2003. ©ASCE, ISSN 0733-9445/2003/6-717–724/$18.00.

$$f_{c1m}=\sum_{i=1}^{m}\rho_i(f_{scr,i}-f_{sm,i})\cos^2\theta_i\leqslant\sum_{i=1}^{m}\rho_i(f_{sy,i}-f_{sm,i})\cos^2\theta_i \quad (1)$$

The subscript "i" indicates a reinforcement component ($i=1$ to m). The concrete stress f_{c1m} is limited by the yield stress of the reinforcement, f_{sy}. The DSFM adopts three assumptions in order to determine the local stress f_{scr}. First, the average tensile concrete stress f_{c1m} is given as a function of principal tensile strain ε_1. The newest model for this function was derived from the work of Bentz (Bentz 1999) as follows:

$$f_{c1m}=\frac{f_t'}{1+\sqrt{\dfrac{2.2\varepsilon_1}{\Sigma_{i=1}^{m}\dfrac{\rho_i}{d_{bi}}|\cos\theta_i|}}} \quad (2)$$

The second assumption deals with the reinforcement ratio ρ. If the reinforcement is uniformly distributed in a cross section of concrete, then the ratio ρ is simply given by A_s/A_c, where A_s and A_c are cross-sectional areas of the reinforcement and concrete, respectively. In actual structures subjected to strengthening or rehabilitation with a FRP sheet, however, large parts of cross sections are often concrete containing very small amounts of reinforcement. In the practice of finite element modeling, an effective reinforcement ratio $\rho_e=A_s/A_{ce}$ should be determined. It is commonly accepted that the effective concrete area A_{ce} is a zone of concrete within approximately 7-1/2 bar diameters from the reinforcement or less ($R_e\leqslant 7.5d_b$), as suggested by the CEB-FIP model code (CEB-FIP 1978).

Third, the DSFM also adopts a model based on the CEB-FIP model code in order to estimate the crack spacing in cracked reinforced concrete. This model is a function of cross-sectional area ratio, diameter, and spacing of reinforcements as expressed by Eq. (3)

$$s_r=(c_s+s_s/10)+0.1d_b/\rho \quad (3)$$

where c_s = distance between reinforcing bars and the centroid of a member, and s_s = spacing of reinforcements. So far, combinations of the above three models have provided accurate predictions of behavior for RC members (Vecchio 2000, 2001a,b). All of the above models related to the tension stiffening effects and crack formation, however, have been derived from experiments of conventional steel-reinforced concrete and are not applicable to the RC with an externally bonded FRP sheet. The objective of this study is the further development of the models, taking into account the influences of both steel bars and the FRP sheet.

Bond Test between Fiber-Reinforced Polymer Sheet and Concrete

An experimental program was conducted in order to derive the bond stress-slip relationship between a FRP sheet and concrete. Fig. 1 shows the geometry of the specimen. The specimen consisted of a 800 mm long concrete block with a 100 mm × 100 mm cross section. FRP sheets with 50 mm width were bonded onto the lateral sides of the block. The blocks had grooves at the center; to which a crack was induced before loading. Tension was applied to the deformed bars embedded in the block. The bars were cut on the center so that the FRP sheets exclusively carried the tension force. The longitudinal sheets were wrapped by a transverse sheet on the left half of the specimen in order to force the sheet to peel only on the right half. The sheet length L was varied between 100, 200, and 400 mm and two specimens were prepared for each length (Table 1). The FRP used consisted of carbon fiber and epoxy resin. The average thickness t_F, elastic modulus E_F, and tensile strength of the FRP were 0.84 mm, 99,500 MPa, and 1,090 MPa, respectively. The compressive strength of the concrete cylinders was 31.9 MPa. All the specimens failed by peeling of the FRP sheets. Distribution of the FRP sheet strain was assumed as Fig. 1 shows in order to estimate the slip S_F between the sheet and the concrete. According to this assumption, the S_F is given by

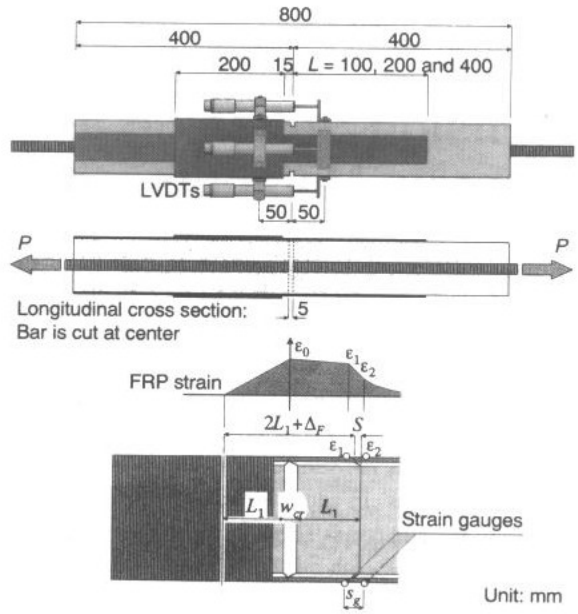

Fig. 1. Geometry of bond test specimen and FRP strain distribution

$$S_F=w_{cr}-\Delta_F \quad (4)$$

$$\Delta_F=\varepsilon_0L_1/2+(\varepsilon_0+\varepsilon_1)(L_1-s_g/2)/2+(\varepsilon_1+\varepsilon_2)s_g/2 \quad (5)$$

$$\varepsilon_0=P/(2w_Ft_FE_F) \quad (6)$$

where w_{cr} = crack width at the center; Δ_F = elongation of the FRP sheet; ε_1, ε_2 = measured sheet strain (Fig. 1); w_F = width of a sheet = 50 mm; L_1 = half LVDT-gauge length = 50 mm (Fig. 1); P = tension force applied to the specimen; and s_g = spacing of strain gauges = 15 mm. The bond stress τ_{bF}, which corresponds to slip S_F, is given by

$$\tau_{bF}=w_Ft_FE_F(\varepsilon_1-\varepsilon_2)/(w_Fs_g) \quad (7)$$

Typical relations between the bond stress τ_{bF} and the slip S_F are shown in Fig. 2(a). The τ_{bF}-S_F curve possesses a tension-softening-like shape for concrete in tension. The area enveloped by the curve is defined as fracture energy of the bonded area, G_f.

Table 1. Bond Test

Specimen	L (mm)	P_{max} (kN)	G_f (N/mm)
T1-1	100	15.8	0.150
T1-2		19.4	0.226
T2-1	200	21.7	0.282
T2-2		26.4	0.376
T4-1	400	26.3	0.373
T4-2		23.3	0.326

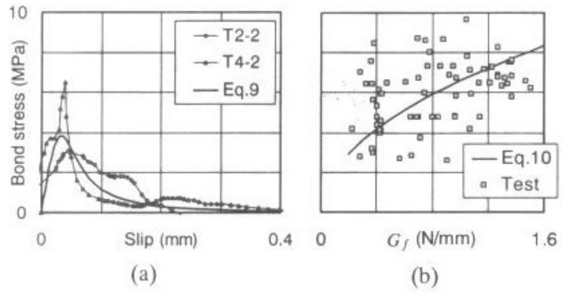

Fig. 2. Comparison between tests and models of FRP bond and (a) bond stress-slip relations; (b) bond stress-fracture energy relations

The Recommendation of JSCE provides a theoretical equation for the fracture energy G_f as defined in Eq. (8) (JSCE 2001).

$$G_f = P_{\max}^2/(8w_F^2 t_F E_F) \tag{8}$$

The average value for the G_f, in this test, was 0.39 N/mm.

Relationship between Bond Stress and Slip

Nakaba et al. (2001) proposed the bond stress-slip relation expressed in Eqs. (9) to (11).

$$\frac{\tau_{bF}}{\tau_{bFy}} = \frac{S_F}{S_{Fy}} \cdot \frac{3}{2+(S_F/S_{Fy})^3} \tag{9}$$

where

$$\tau_{bFy} = 6.6\sqrt{G_f} \qquad \text{(MPa)} \tag{10}$$

$$S_{Fy} = 0.057\sqrt{G_f} \qquad \text{(mm)} \tag{11}$$

where units of G_f=N/mm. A curve for the case of G_f =0.39 N/mm, which corresponds to the test result in this study, is drawn in Fig. 2(a). The maximum bond stress was originally given by $\tau_{bFy}=3.5f_c'^{0.19}$ (MPa) and the slip by $S_{Fy}=0.065$ mm in the work of Nakaba et al. The τ_{bFy}, however, considerably varies depending on the bonding condition even when the concrete strength f_c' is the same. For instance, the τ_{bFy} in the test of Sato and Kimura (Sato et al. 1997b) ($f_c'=37.6$ MPa) was 4.56 MPa, which was approximately two-thirds the value estimated by $3.5f_c'^{0.19}$. In addition, Ueda et al. (1997) suggested that the τ_{bFy} also depends on the stiffness of the FRP sheet. Eq. (10) is therefore used as the relation between τ_{bFy} and G_f in this study [Fig. 2(b)]. The writers are continuing further research to make a more reliable model for the τ_{bFy}-G_f relation.

Equilibrium and Compatibility Conditions of Bond

This section presents equilibrium and compatibility formulations for the bond between concrete and reinforcement, required in order to undertake a parametric analysis of the tension stiffening effect and crack formation. The compatibility condition of the bond between the reinforcement and concrete shown in Fig. 3(a) provides Eq. (12).

$$\frac{dS(u_1)}{du_1} = \frac{\varepsilon_s(u_1)-\varepsilon_c(u_1)}{\cos\theta_s} \tag{12}$$

where S=slip between the reinforcement and concrete; u_1 =coordinate along the principal tensile concrete stress direction; θ_s=angle between the reinforcement and principal tensile con-

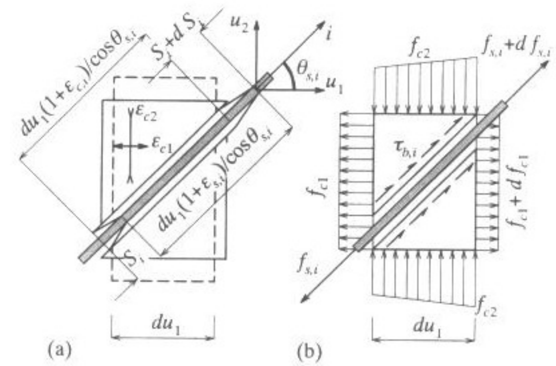

Fig. 3. Bond between concrete and reinforcements: (a) compatibility (ith bar) and (b) equilibrium (ith bar)

crete stress direction; ε_s=reinforcement strain; and ε_c =concrete strain along the reinforcement axis. On the other hand, the equilibrium condition shown in Fig. 3(b) results in Eq. (13).

$$\tau_b(u_1) = \frac{A_s\cos\theta_s}{\psi_s}\frac{df_s(u_1)}{du_1} \tag{13}$$

where τ_b=bond stress between the reinforcement and concrete and ψ_s=bonded area per unit length (mm^2/mm). The stress-strain relation of the reinforcement is modeled as a bilinear relation expressed by Eq. (14).

$$f_s(u_1) = E_s\varepsilon_s(u_1) \quad [\varepsilon_s(u_1)\leq\varepsilon_{sy}] \tag{14a}$$

$$f_s(u_1) = f_{sy}+E_{sh}[\varepsilon_s(u_1)-\varepsilon_{sy}] \quad [\varepsilon_{sy}<\varepsilon_s(u_1)] \tag{14b}$$

In the case of FRP, the plastic range expressed by Eq. (14b) does not exist. The equilibrium between the concrete strain ε_c and the bond stress τ_b is given by Eq. (15).

$$\frac{d\varepsilon_c(u_1)}{du_1} = \sum_{i=1}^{m}\left(-\frac{\psi_{s,i}\cos\theta_{s,i}\tau_{b,i}(u_1)}{A_{ce}E_c}\right) \tag{15}$$

where A_{ce}=effective cross-sectional area of concrete. The differential equilibrium and compatibility conditions expressed by Eq. (16) are derived from Eqs. (12) to (15).

$$\frac{d^2S_i(u_1)}{du_1^2} = \frac{1}{\cos\theta_{s,i}}\left\{\frac{\psi_{s,i}\tau_{b,i}(u_1)}{A_{s,i}E'_{s,i}} + \sum_{i'=1}^{m}\left(\frac{\psi_{s,i'}\cos\theta_{s,i'}\tau_{b,i'}(u_1)}{A_{ce}E_c}\right)\right\} \tag{16}$$

where $E_s'=E_s$ for $\varepsilon_s(u_1)\leq\varepsilon_{sy}$ and $E_s'=E_{sh}$ for $\varepsilon_{sy}<\varepsilon_s(u_1)$. For numerical calculation, Eq. (16) can be discretized as expressed by Eq. (17).

$$\frac{dS_i(u_{1,k+1})}{du_1} = \frac{dS_i(u_{1,k})}{du_1} + \frac{\Delta u_1}{\cos\theta_{s,i}}\left[\frac{\psi_{s,i}\tau_{b,i}(u_{1,k})}{A_{s,i}E'_{s,i}} + \sum_{i'=1}^{m}\left(\frac{\psi_{s,i'}\cos\theta_{s,i'}\tau_{b,i'}(u_{1,k})}{A_{ce}E_c}\right)\right] \tag{17a}$$

$$S_i(u_{1,k+1}) = S_i(u_{1,k}) + \Delta u_1\frac{dS_i(u_{1,k})}{du_1} \tag{17b}$$

where subscript "k" represents a discretized location along u_1 coordinate. The reinforcement stress is calculated by Eq. (18).

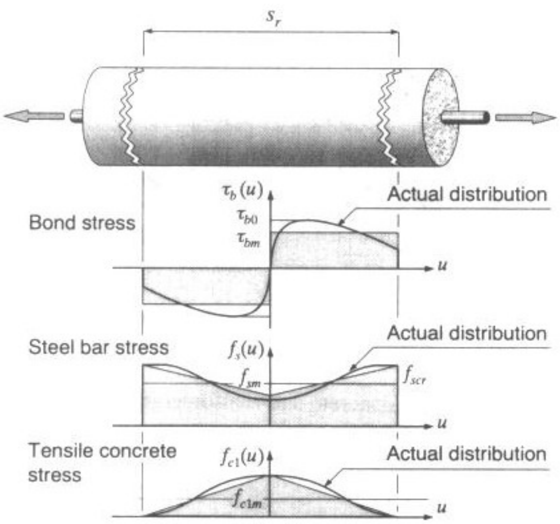

Fig. 4. Tension chord with steel bar

$$f_s(u_1)=\frac{\psi_s}{A_s\cos\theta_s}\int_0^{u_1}\tau_b(u_1)du_1+f_{s0} \tag{18}$$

where f_{s0} = reinforcement stress at the midpoint between cracks. The tensile concrete stress is given by Eq. (19).

$$f_{c1}(u_1)=\sum_{i=1}^{m}\left(-\int_0^{u_1}\frac{\psi_{s,i}\cos\theta_{s,i}\tau_{b,i}(u_1)}{A_{ce}}du_1\right)+f_{c10} \tag{19}$$

When the tensile concrete stress at the midpoint between cracks f_{c10} reaches the tensile concrete strength f_t', a crack occurs. Eqs. (17) to (19) should satisfy the compatibility condition of the average strain between cracks expressed by Eq. (20).

$$2S_{cr}+s_r\varepsilon_{c1m}=s_r\varepsilon_s\cos^2\theta_s \tag{20}$$

where S_{cr} = bond slip at the crack; ε_{c1m} = average tensile concrete strain; and ε_{sm} = average reinforcement strain. The crack spacing and tension stiffening effect can be evaluated by solving Eqs. (17) to (20) numerically. In practice, however, it is not realistic to conduct these calculations for each set of reinforcement at every crack in the FE analysis. For the sake of simplification, the equations for crack spacing and tension stiffening effect will be proposed based on parametric calculations in the following sections.

Modeling the Contribution of a Steel Bar to Crack Formation

This study adopts the concept of the tension chord employed by Kaufmann and Marti (Kaufmann and Marti 1998) shown in Fig. 4 in order to estimate the contribution of steel bars to the crack formation. Eq. (21) provides the equilibrium between tensile concrete strength and the bond stress at the final crack formation.

$$f_1'=\sum_{i=1}^{n}\frac{s_r\psi_{s,i}\tau_{b0,i}\cos\theta_{s,i}}{2A_{ce}} \tag{21}$$

where $\tau_{b0,i}$ = maximum average bond stress of ith steel bar. In this model, τ_{b0} is assumed to be $2f_t'$ as suggested by Kaufmann.

Modeling the Tension Stiffening Effect of a Steel Bar

In order to model the tension stiffening effect of steel bars, parametric analyses were conducted for 16 cases of the tension chord

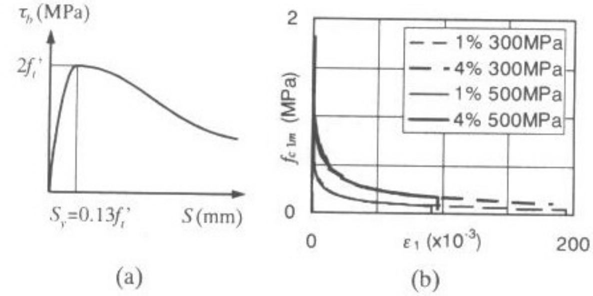

Fig. 5. Analysis of tension-stiffening effects: (a) assumed τ_b-S relation and (b) analyzed f_{c1m}-ε_1 relations

with varied stress-strain relations, bar diameters d_b, reinforcement ratio ρ, and angle of steel bars θ_s as follows:

1. $f_s-\varepsilon_m$ relation: $(f_{sy}, f_{su}, \varepsilon_{su})$ = (300 MPa, 450 MPa, 0.1) or (500 MPa, 625 MPa, 0.05)
2. d_b: 10 mm or 30 mm
3. ρ: 1% or 4%
4. θ_s: 0° or 45°

Fig. 5(a) shows the assumed local bond stress-slip relation between steel and concrete given by Eq. (22) (Muguruma et al. 1967).

$$\frac{\tau_b}{2f_t'}=e\,\frac{\ln\{(e-1)S/S_y+1\}}{(e-1)S/S_y+1} \tag{22}$$

where S_y = slip at the maximum bond stress = $0.13f_t'$ (mm). The compressive strength was assumed to be 26 MPa and the tensile strength by $f_t'=0.33\sqrt{f_c'}=1.7$ MPa. Fig. 5(b) shows typical analyzed relations between the average tensile concrete stress f_{c1m} and the principal tensile strain ε_1 for d_b = 30 mm, θ_s = 45°, f_{sy} = 300 MPa, or 500 MPa and ρ = 1 or 4%. As Fig. 5(b) shows, the variation of the stress-strain relation of the steel had no influence on the $f_{c1m}-\varepsilon_1$ relations although the other variables d_b, ρ, and θ_s did.

Herein modeling of the tension stiffening effect and the crack formation is conducted introducing the concept of "average bond." Fig. 6(a) shows all the analyzed relationships between normalized average bond stress τ_{bm}/f_t' and the average bond slip S_{sm} defined by Eq. (23).

$$S_m=\varepsilon_{sm}s_r/(2\cos\theta_s) \tag{23}$$

where ε_{sm} = average strain of the steel bar. The average bond slip S_m is equal to elongation of the steel bar over a one-half crack spacing. Despite wide variations in the $f_s-\varepsilon_s$ relation, the diam-

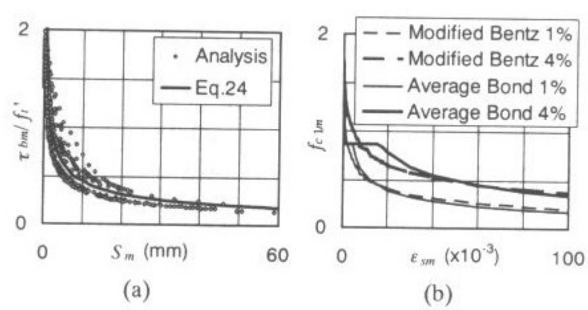

Fig. 6. Modeling of tension-stiffening effect of steel bar: (a) average bond model and (b) modeled f_{c1m}-ε_m curves

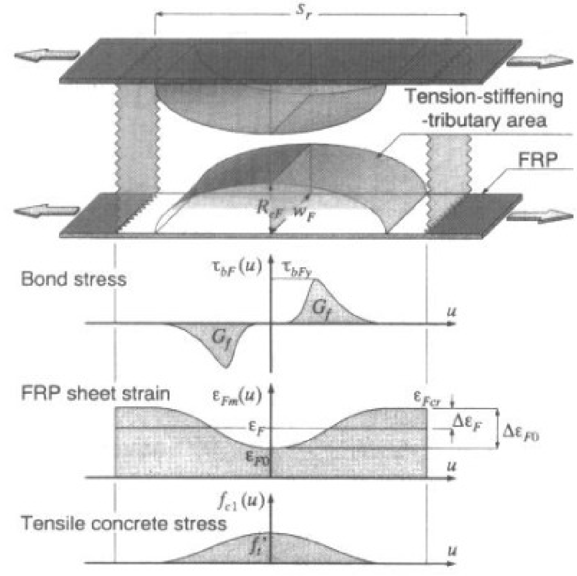

Fig. 7. Tension chord with FRP sheet

eter d_b, the reinforcement ratio ρ, and the angle θ_s, the analyzed data indicate a single trend in the $\tau_{bm}/f_t' - S_m$ relation. Eq. (24) provides a best fit to this trend.

$$\tau_{bm}=\tau_{b0}\sqrt{\frac{1}{2S_m}}=\tau_{b0}\sqrt{\frac{\cos\theta_s}{s_r\varepsilon_{sm}}}\leqslant\tau_{b0} \qquad \text{(MPa)} \qquad (24)$$

Average tensile concrete stress is given by Eq. (25).

$$f_{c1m}=\sum_{i=1}^{n}\frac{s_r\psi_{s,i}\tau_{bm,i}\cos\theta_{s,i}}{2A_{ce,i}}=s_r\tau_{b0}\sum_{i=1}^{n}\left\{\frac{\rho_i\cos\theta_{s,i}}{d_{b,i}}\times\min\left(1,\sqrt{\frac{\cos\theta_{s,i}}{s_r\varepsilon_{sm}}}\right)\right\} \qquad \text{(MPa)} \qquad (25)$$

Fig. 6(b) compares $f_{c1m}-\varepsilon_s$ relations between the average bond model and the modified Bentz model (d_b = 10 mm, f_{sy} = 300 MPa, $\theta_s = 0°$, and ρ = 1 or 4%).

Modeling the Contribution of Fiber-Reinforced Polymer to Crack Formation

Fig. 7 shows a tension chord model of concrete with the FRP sheets. The symbol $\Delta\varepsilon_{F0}$ represents the difference between the minimum strain ε_{F0} and the maximum strain at crack ε_{Fcr}. When the concrete stress reaches the tensile strength f_t' at midpoint between cracks, then a new crack develops at this section. Eq. (26) expresses the equilibrium at the new crack formation.

$$f_t'=\sum_{j=1}^{n}\frac{w_{F,j}t_{F,j}E_{F,j}\Delta\varepsilon_{F0,j}\cos^2\theta_{F,j}}{A_{ce}} \qquad (26)$$

Using Eqs. (17)–(20) and (26), relationships between $\Delta\varepsilon_{F0}$ and the average FRP strain ε_F were calculated for the tension chords of a series of FRP sheets with variable s_r, $t_F E_F$, and G_f. Note that the variables f_s, τ_b, ψ_s, θ_s, S, and ε_s in Eqs. (17) to (20) are replaced by f_F, τ_{bF}, ψ_F, θ_F, S_F, and ε_F. Variation of s_r, $t_F E_F$, and G_f are as follows:

- s_r = 32, 80, 200, and 500 mm,
- $t_F E_F$ = 20,000, 40,000, 60,000, and 80,000 N/mm, and
- G_f = 0.4, 0.8, 1.2, and 1.6 N/mm

The reinforcement ratio ρ_F was not included as a parameter in these calculations because the stiffness of the FRP sheet is usually negligibly small relative to that of the concrete (i.e., $w_F t_F E_F \ll A_c E_c$). Fig. 8(a) presents differences between the maximum and the minimum tensile FRP forces per unit width $t_F E_F \Delta\varepsilon_{F0}$ with respect to the average strain ε_{Fm} for the case of $t_F E_F$ = 80,000 N/mm and G_f = 0.40 N/mm. The term $t_F E_F \Delta\varepsilon_{F0}$ achieves the maximum at a ε_{Fm} less than 0.01. The crack formation will occur in most RC members when this range of strain is achieved. It is therefore sufficient to evaluate only the maximum of the $t_F E_F \Delta\varepsilon_{F0}$ term in order to estimate the crack spacing. Eq. (27) provides the best fit to $t_F E_F \Delta\varepsilon_{F0\,\max}$ based on the analysis of the tension chords. Fig. 8(b) compares the analyzed and the fitted relations between the $t_F E_F \Delta\varepsilon_{F0\,\max}$ and the crack spacing s_r.

$$t_F E_F \Delta\varepsilon_{F0\,\max}=c_3\times\min(1, s_r/220) \qquad \text{(N/mm)} \qquad (27)$$

where

$$c_3=(15.8+1.34\sqrt{t_F E_F})\sqrt{G_f} \qquad \text{(N/mm)} \qquad (28)$$

The units of s_r, t_F, E_F, and G_f are mm, mm, MPa, and N/mm, respectively. When the average tensile stress in the cross-section of $R_{eF}\times w_F$ (Fig. 7) at the midpoint between cracks approaches the tensile strength f_t', then a new crack develops at this section. Eq. 29 gives the possible maximum depth R_{eF}.

$$R_{eF}=\frac{1}{f_t'}\sum_{j=1}^{n}(15.8+1.34\sqrt{t_{F,j}E_{F,j}})\sqrt{G_{f,j}} \qquad \text{(mm)} \qquad (29)$$

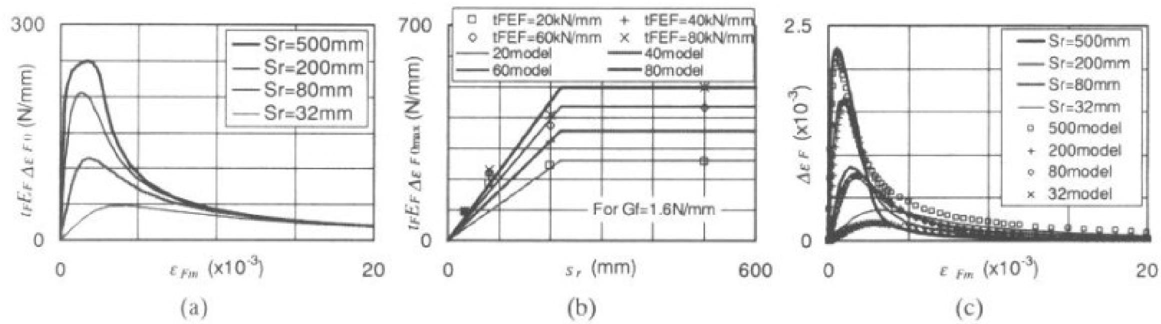

Fig. 8. Models for crack formation and tension-stiffening effect of RC with FRP: (a) $t_F E_F \Delta\varepsilon_{F0\,\max}-\varepsilon_{Fm}$ relations and (b) $t_F E_F \Delta\varepsilon_{F0\,\max}-s_r$ relations; (c) modeling $\Delta\varepsilon_F-\varepsilon_{Fm}$ relations

Table 2. Specifications of RWOA Beams

Beam	f_c (MPa)	f'_t (MPa)	Bottom bars	Span (mm)	Section (mm)	Fiber-reinforced polymers	τ_{bFy} (MPa)	S_{Fy} (mm)	S_{Fu} (mm)	V_{exp} (kN)
RWOA1	22.6	1.57	2-30ϕ+2-25ϕ	3,660	305×560	w200 mm @300 mm	3.86	0.033	0.177	492.6
RWOA2	25.9	1.69	3-30ϕ+2-25ϕ	4,570			3.96	0.034	0.182	458.7
RWOA3	43.5	2.18	4-30ϕ+2-25ϕ	6,400			4.37	0.038	0.201	436.2

Modeling the Tension Stiffening Effect of Fiber-Reinforced Polymers

The tension stiffening effect of the FRP sheet is defined by the difference between the average stress f_{Fm} and the local stress at cracks f_{Fcr}. Based on the calculations in the previous section, the strain difference $\Delta\varepsilon_F=(f_{Fcr}-f_{Fm})/E_F$ was modeled by a curve expressed by Eqs. (30)–(34)

$$\frac{\Delta\varepsilon_F}{\Delta\varepsilon_{F\max}}=\frac{\varepsilon_{Fm}}{\varepsilon_{F1}}\cdot\frac{\alpha}{(\alpha-1)+(\varepsilon_{Fm}/\varepsilon_{F1})^{\alpha}} \quad (30)$$

where

$$\Delta\varepsilon_{\max}=\sqrt{G_f}\left[\frac{1{,}340}{\sqrt{t_F E_F}}-1.27-\left\{c_2\left(\frac{s_r}{\cos\theta_F}-640\right)\right\}^4\right]\times 10^{-3} \quad (31)$$

$$\varepsilon_{F1}=\sqrt{G_f}\left\{\left(25+\frac{185{,}000}{t_F E_F}\right)\sqrt{\frac{\cos\theta_F}{s_r}}-0.32\right\}\times 10^{-3} \quad (32)$$

$$\alpha=2.7-\left(\frac{s_r}{640\cos\theta_F}\right)^2 \quad (33)$$

$$c_2=\{-3.1+9.3/(t_F E_F)^{0.05}\}\times 10^{-3} \quad (34)$$

The units of s_r, t_F, E_F, and G_f are again mm, mm, MPa, and N/mm, respectively. Fig. 8(c) presents typical relationships between $\Delta\varepsilon_F$ and ε_{Fm} for case of $t_F\ E_F=80{,}000$ N/mm and $G_f=0.40$ N/mm with varied crack spacing s_r. The $\Delta\varepsilon_F$ is proportional to average tensile concrete stress f_{c1m} (i.e., $f_{c1m}=w_F t_F E_F \Delta\varepsilon_F/A_c$) while the ε_{Fm} is equal to the average tensile strain ε_1 (i.e., $\varepsilon_1=\varepsilon_{Fm}$). Therefore, Fig. 8(c) is another expression of the tension stiffening curve. The $\Delta\varepsilon_F$ increases as the average strain ε_{Fm} increases, but soon begins to decrease due to debonding.

Combining Models

Referring to Eqs. (21) and (26), the equilibrium condition at completion of the crack formation in a RC member comprised of steel bars and FRP sheets can be expressed by Eq. (35).

$$f'_t=2s_r\sum_{i=1}^{m}\frac{\rho_{e,i}\tau_{s0,i}\cos\theta_{s,i}}{d_{b,i}}+\sum_{j=1}^{n}\rho_{F,j}E_{F,j}\Delta\varepsilon_{F\max,j}\cos^2\theta_{F,j} \quad (35)$$

where ρ_e = effective reinforcement ratio for the steel bars and ρ_F = effective reinforcement ratio for the FRP sheet $=t_F/R_{eF}$. The subscript "i" indicates a component (direction) of steel bars ($i=1$ to m), while the "j" denotes a component of FRP sheets ($j=1$ to n). The coefficient $c_{3,j}$ is given by Eq. (28). Eq. (36) gives the crack spacing.

$$s_r=\frac{f'_t}{2\Sigma_{i=1}^{m}\dfrac{\rho_{c,i}\tau_{b0,i}\cos\theta_{s,i}}{d_{b,i}}+\dfrac{1}{220}\Sigma_{j=1}^{n}\dfrac{\rho_{F,j}c_{3,j}\cos^2\theta_{F,j}}{t_{F,j}}} \quad (s_r\leqslant 220\text{ mm}) \quad (36a)$$

$$s_r=\frac{f'_t-\Sigma_{j=1}^{m}\dfrac{\rho_{F,j}c_{3,j}\cos^2\theta_{F,j}}{t_{F,j}}}{2\Sigma_{i=1}^{n}\dfrac{\rho_{e,i}\tau_{b0,i}\cos\theta_{s,i}}{d_{b,i}}} \quad (s_r>220\text{ mm}) \quad (36b)$$

The calculations of the crack spacing will be reduced without remarkable deterioration of accuracy if the s_r is replaced by s'_r expressed by Eqs. (37)–(39).

$$s'_r=\frac{\lambda}{\dfrac{\sin\theta}{s_{rx}}+\dfrac{\cos\theta}{s_{ry}}} \quad (37)$$

where

$$s_{rx}=s_r(\theta_{s,i}=\theta_{sx,i},\theta_{F,i}=\theta_{Fx,i}) \quad (38)$$

$$s_{ry}=s_r(\theta_{s,i}=\theta_{sy,i},\theta_{F,i}=\theta_{Fy,i}) \quad (39)$$

λ = crack formation parameter = 0.75; θ = angle between horizontal axis (x axis) and the principal tensile stress direction; $\theta_{sx,i}$ = angle between horizontal axis (x axis) and ith component of steel bars; $\theta_{sy,i}$ = angle between vertical axis (y axis) and ith component of steel bars; $\theta_{Fx,j}$ = angle between horizontal axis (x axis) and jth component of FRP sheets; and $\theta_{Fy,j}$ = angle between vertical axis (y axis) and jth component of FRP sheets.

The parameter s_{rx} is equal to the crack spacing in the case where the principal tensile stress direction and the x axis coincide, while the s_{ry} is equal to that where the principal tensile stress direction and the y axis coincide. Eq. (37) interpolates the actual crack spacing in each loading stage between s_{rx} and s_{ry}. When the crack pattern has stabilized, the crack spacing is equal to or less than twice the length over which slip between reinforcement and concrete occurs. The final crack spacing therefore becomes either s_r or $0.5s_r$. The above-defined crack formation parameter $\lambda=0.75$ provides an average between the two.

Eq. (40) gives the average tensile concrete stress induced by the steel bars and the FRP sheets.

$$f_{c1m}=s'_r\tau_{b0}\sum_{i=1}^{m}\left\{\frac{\rho_{e,i}\cos\theta_{s,i}}{d_{b,i}}\times\min\left(1,\sqrt{\frac{\cos\theta_{s,i}}{s_r\varepsilon_{sm}}}\right)\right\}+\sum_{j=1}^{n}\rho_{F,j}E_{F,j}\Delta\varepsilon_F\cos^2\theta_{F,j}\quad(\text{MPa}) \quad (40)$$

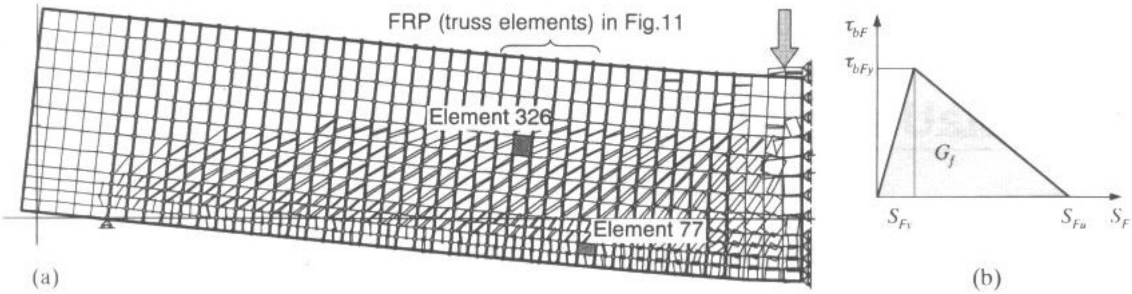

Fig. 9. FE modeling of RWOA beams: (a) FE model (RWOA1/Case 2, disp. = 33.2 mm); (b) bilinear modeling of bond stress-slip relation for FRP

Example Analyses

The proposed models for crack spacing and tension stiffening effect were implemented into a nonlinear FE program *VecTor2*. This section describes calculations for example RC beams with externally bonded FRP sheets. Table 2 provides the specifications for Beams RWOA1, RWOA2, and RWOA3 considered here (Wong 2001). The cross section of the beams was 305 mm $\times$ 560 mm and the spans varied between 3,660, 4,570, and 6400 mm. The FRP sheets, which were the same as those used in the bond test, were cut into 200 mm widths and were applied at a 300 mm spacing. The sheets were not wrapped around the cross section nor anchored, but only bonded to the lateral sides of the beams to allow observation of peeling. The beams were subjected to three-point loading and each failed by crushing at the loading point after the bottom longitudinal steel bars had yielded. After yielding, peeling of the FRP sheets was observed near the loading point. The FRP sheets abruptly split off as the concrete crushed.

The beams were modeled for FE analysis taking advantage of symmetry to model half-spans as Fig. 9(a) shows. A mesh of 43 $\times$ 12 constant strain (eight degrees of freedom) rectangular elements were used for Beam RWOA1, 53$\times$12 elements for Beam RWOA2, and 68$\times$10 elements for Beam RWOA3. The bottom steel bars and the FRP sheets were modeled by truss elements. The bond between concrete and the FRP sheets were represented by four-node joint elements. Fig. 9(b) shows a bilinear simplification of the bond stress-slip relation obtained from the corresponding bond test. The maximum bond stress τ_{bFy} was adjusted based on an assumption that the τ_{bFy} is proportional to $f_c'^{0.19}$ (Table 2). The characteristic slips S_{Fy} and S_{Fu} were also modified through Eqs. (10) and (11). The beams were subjected to displacement-control loading, with midspan displacement increments of 2 mm imposed.

Two series of calculations were conducted for each beam. Case 2 adopts the proposed models in this study, while Case 1 calculations used the modified Bentz model for the tension stiffening effects of steel bars and the CEB-FIP model code for the crack spacings. With Case 1, the tension stiffening effects of the FRP and the contribution of the FRP to the crack formation were neglected since these are out of range of the modified Bentz model and the CEB-FIP model code. Fig. 10 compares the experimental and the analytical relationships between shear force and the midspan displacement. The macroresponses in Fig. 10 indicate slight differences between Case 2 and Case 1 results.

Table 3 compares experimental and analytical crack widths in typical locations of Beam RWOA1. The locations of the corresponding FE elements are indicated in Fig. 9(a). In Element 77, which is located at the bottom near the center of the beam, Case 2 analysis estimated the crack width at 0.71 mm and Case 1 at 0.62 mm while the test-observed value was 0.90 mm. The estimates of the two cases for this element seem reasonable since crack spacings usually vary by 50 to 200%. In Element 326, which is located at the mid-depth of the beam, the crack width observed in the test was 0.20 mm. For this element, Case 2 analysis estimated the width at 0.46 mm, while Case 1 gave 2.24 mm. The former seems reasonable while the latter is an obvious overestimation because of the neglect of the contribution of the FRP to the crack formation.

Fig. 11 compares distributions of average and local strains of the FRP sheets at the maximum shear of RWOA1. A strain distribution of each column of the truss elements is shifted with every 3×10^{-3} strain. Fig. 11(b) shows Case 2 results. Remarkable differences between the local and the average strains were observed. The effective depths for tension stiffening effect R_{eF} of Beams RWOA1, RWOA2, and RWOA3 were estimated at Eq. (29) at 136, 133, and 112 mm respectively. These areas resulted in

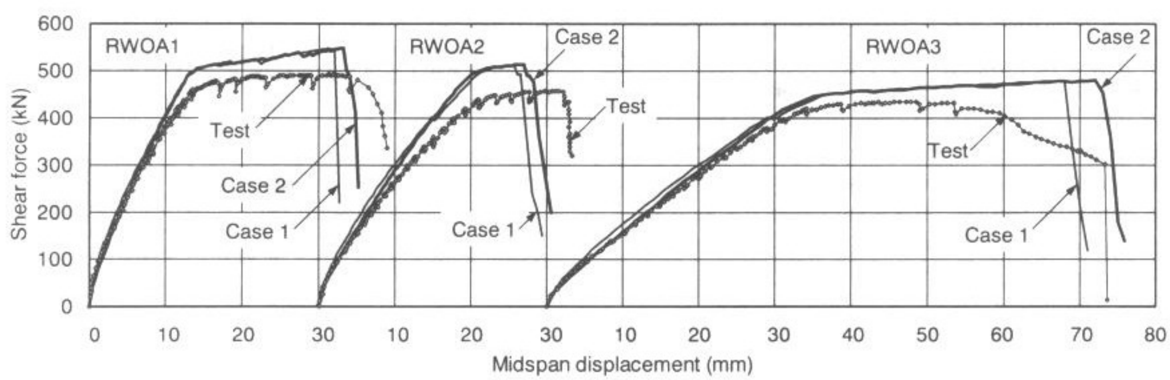

Fig. 10. Load-deflection relations of RWOA beams

Table 3. Comparison of Crack Widths of Beam RWOA1

Element number	Case 1	Case 2	Test
77	0.62 mm	0.71 mm	0.90 mm
326	2.24 mm	0.46 mm	0.20 mm

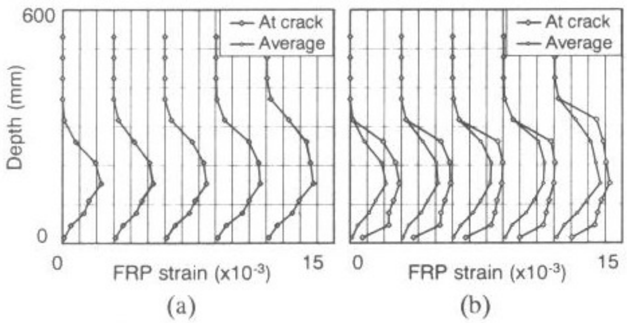

Fig. 11. Average and local strains of FRP sheet of Beam RWOA1: (a) Case 1 and (b) Case 2

differences between the local and the average strains from 1×10^{-3} up to 2×10^{-3}. In Case 1 analysis, on the other hand, the neglect of the tension stiffening effect of the FRP resulted in the entire coincidence of the local strains with the average as Fig. 11(a) shows. This is obviously not the case in the actual beams where the local FRP strain must considerably increase at cracks.

These analyses indicated that the proposed models are an effective tool for the estimations of crack widths and tension stiffening effects in RC members with externally bonded FRP sheets, which were out of the range of the existing models.

Conclusions

Analytical models for crack formation and tension stiffening effect, for steel bars, and an externally bonded FRP sheet, were developed based on considerations of the bond characteristics between the two reinforcement types and concrete. These models were combined with the DSFM in the algorithm of a nonlinear finite-element method. The following are the characteristic aspects of these models:

1. The concept of average bond was introduced for modeling the tension stiffening effect of steel bars. The average bond model considers gradual propagation of the bond deterioration and enables a combination with models related to the FRP sheets;
2. The tension stiffening effect of the FRP is independent on the cross-sectional area of concrete because the stiffness of the FRP is usually negligible relative to that of concrete. Nevertheless, the FRP contributes to the crack formation of the RC members to a certain extent. The proposed model estimates these characteristics of the FRP considering the potential peeling from concrete; and
3. The models enable one to estimate the combined contributions of the steel bars and the FRP sheet to the crack formation and tension stiffening effects.

The models successfully overcame the limitations of the existing models and thus extended the ability of the DSFM. Since the corroborating analyses were conducted for beams that failed by flexural crushing, the model should be corroborated in future research by application to other members whose failures are governed by peeling or rupture of the FRP sheet.

Acknowledgments

The writers' grateful appreciation goes to Professor Shamim A. Sheikh, Professor Evan Bentz, and Ms. Rita Wong of University of Toronto for their assistance. Professor Bunzo Tsuji and Professor Shigeru Fujii of Kyoto University, Japan, are acknowledged for providing the opportunity of this research. The FRP materials were provided by R. J. Watson Inc. and Fyfe Company.

References

Bentz, E. C. (1999). "Sectional analysis of reinforced concrete structures." PhD thesis, Dept. of Civil Engineering, Univ. of Toronto, Toronto.

Comité Euro-International du Beton-Fédération International de la Precontrainte (CEB-FIP). (1978). *Model code for concrete structures: CEB-FIP international recommendations*, 3rd Ed., Comité Euro-International du Béton, Paris, 348.

Japanese Society of Civil Engineering (JSCE). (2001). "Recommendations for upgrading of concrete structures with use of continuous fiber sheets." Japanese Society of Civil Engineering, Tokyo, Japan.

Kaufmann, W., and Marti, P. (1998). "Structural concrete: Cracked membrane model." *J. Struct. Eng.*, 124(12), 1467–1475.

Muguruma, H., Morita, S., and Tomita, K. (1967). "Fundamental study on bond between steel and concrete." *J. Arch. Inst. Jpn.*, 131, 1–8, (in Japanese).

Nakaba, K., Kanakubo, T., Furuta, T., and Yoshizawa, H. (2001). "Bond behavior between fiber-reinforced polymer laminates and concrete." *ACI Struct. J.*, 98(3), 359–367.

Sato, Y., Katsumata, H., and Kobatake, Y. (1997a). "Shear strengthening of existing reinforced concrete beams by CFRP sheet." *Proc., 3rd Int. Symposium FRP Reinforcement for Concrete Structures*, Japan Concrete Institute, Spporo, Japan, 507–514.

Sato, Y., Kimura, K., and Kobatake, Y. (1997b). "Bond behavior between CFRP sheet and concrete (Part 1)." *J. Struct. Const. Eng., Arch. Inst. Jpn.*, 500, 75–82.

Ueda, T., Sato, Y., and Asano Y. (1999). "Experimental study on bond strength of continuous carbon fiber sheet." *Proc., 4th Int. Symposium FRP Reinforcement for Concrete Structures*, American Concrete Institute, Detroit, 407–416.

Vecchio, F. J. (2000). "Disturbed stress field model for reinforced concrete: Formulation." *J. Struct. Eng.*, 126(9), 1070–1077.

Vecchio, F. J. (2001a). "Disturbed stress field model for reinforced concrete: Implementation." *J. Struct. Eng.*, 127(1), 12–20.

Vecchio, F. J. (2001b). "Disturbed stress field model for reinforced concrete: Validation." *J. Struct. Eng.*, 127(4), 350–358.

Vecchio, F. J., and Collins, M. P. (1986). "The modified compression-field theory for reinforced concrete elements subjected to shear." *ACI Struct. J.*, 83(2), 219–231.

Wong, R. (2001) "Towards modeling of reinforced concrete members with externally-bonded fibre reinforced polymer (FRP) composites." MASc thesis, Univ. of Toronto, Toronto.